A computational study of magnesium point defects and diffusion in forsterite

Andrew M. Walker, Scott M. Woodley, Ben Slater, Kate Wright

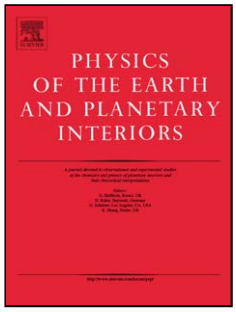

Title: A computational study of magnesium point defects and diffusion in forsterite

Authors: Andrew M. Walker, Scott M. Woodley, Ben Slater, Kate Wright

PII: S0031-9201(08)00058-7
DOI: doi:10.1016/j.pepi.2008.04.001
Reference: PEPI 4919

To appear in: *Physics of the Earth and Planetary Interiors*

Received date: 15-8-2007
Revised date: 19-3-2008
Accepted date: 1-4-2008

Please cite this article as: Walker, A.M., Woodley, S.M., Slater, B., Wright, K., A computational study of magnesium point defects and diffusion in forsterite, *Physics of the Earth and Planetary Interiors* (2007), doi:10.1016/j.pepi.2008.04.001

A computational study of magnesium point defects and diffusion in forsterite

Andrew M. Walker [a,*] Scott M. Woodley [b] Ben Slater [c,d]
Kate Wright [e]

[a] *Department of Earth Sciences, University of Cambridge, Downing Street, Cambridge, CB2 3EQ, UK*

[b] *Davy Faraday Research Laboratory, 3rd Floor, Kathleen Lonsdale Building, University College London, Gower Street, London, WC1E 6BT, UK*

[c] *Department of Chemistry, 20 Gordon Street, UCL, London, WC1H 0AJ, UK*

[d] *Materials Simulation Laboratory, University College London, London, UK*

[e] *Nanochemistry Research Institute, Department of Applied Chemistry, Curtin University of Technology, P.O. Box U1987, Perth 6845, Western Australia*

Abstract

We have studied the formation and migration of point defects within the magnesium sublattice in forsterite using a combination of empirical and quantum mechanical modelling methodologies. Empirical models based on a parameterised force field coupled to a high throughput grid computing infrastructure allow rapid evaluation of a very large number of possible defect configurations. An embedded cluster approach reveals more accurate estimates of defect energetics for the most important defect configurations. Considering all defects in their minimum energy, equilibrium positions, we find that the lowest energy intrinsic defect is the magnesium Frenkel type, where a magnesium atom moves from the M1 site to form a split intersti-

tial defect. This defect has two four coordinated magnesium atoms located outside opposite triangular faces of an otherwise vacant M1 octahedron. The split interstitial defect is more stable than regular interstitials where magnesium is located in either of the two structurally vacant octahedral sites in the hexagonally close packed oxygen lattice. M1 vacancies are also found to form when iron(II) oxidises to iron(III). The energy of the defects away from the equilibrium positions allows the energy barrier to diffusion to be calculated. We have considered the migration of both magnesium vacancies and interstitials and find that vacancies are more mobile. When the contribution from the formation energy of the defects is included we arrive at activation energies for vacancy diffusion that are in agreement with experiment.

Key words: forsterite, olivine, magnesium, defect, diffusion

1 Introduction

Although there is a large body of experimental data pertaining to the diffusion of cations in olivine, there has been no determination of the detailed atomic scale mechanism by which cationic defects form and move through the crystal lattice. Because of the prevalence of olivine in many mafic and ultramafic igneous rocks such basic information is valuable in the extrapolation of laboratory measurements of diffusion for use on a wide variety of geological and geophysical problems. Examples include Fe-Mg exchange in the olivine-spinel mineral pair, which provides an estimate of cooling rates of ultramafic igneous rocks, compositional zoning of olivine crystals growing from a melt, the high

* Corresponding author.
Email address: amw75@cam.ac.uk (Andrew M. Walker).

temperature mechanism of electrical conductivity of the upper mantle, as well as the mantle's viscosity and anelasticity.

As a relatively simple ternary oxide, cation diffusion in olivine is also of interest as a model material for the materials scientist. Chemically it forms a complete solid solution series with compositions ranging between Mg_2SiO_4 (forsterite, Fo_{100}) and Fe_2SiO_4 (fayalite, Fo_0). The iron-free end member is particularly useful in this regard with no significant opportunity for redox chemistry or exchange between the silicon and magnesium sites. Adding iron provides the possibility for the kind of non-stoichiometry that has been extensively studied in binary oxides such as iron and nickel oxide (Dieckmann, 1998) and these processes have been examined in olivine (Smyth and Stocker, 1975; Stocker and Smyth, 1977; Nakamura and Schmalzried, 1983; Tsai and Dieckmann, 1997, 2002).

The olivine structure can be viewed as a distorted hexagonally close packed (HCP) array of oxygen ions with half of the octahederal sites and one eighth of the tetrahedral sites occupied by magnesium or iron ions and silicon atoms, respectively. The distortion of the HCP lattice gives the olivine structure orthorhombic symmetry (space group *Pbnm*) and the unit cell contains four formula units (Figure 1). There are two symmetry distinct octahedral sites: M1, on a centre of symmetry, and M2, on the mirror plane; one distinct tetrahedral site which lies on the mirror plane and three distinct oxygen sites (O1 and O2 on the mirror plane and O3 in a general position). There are also two vacant octahedral sites, I1 on an inversion center and I2 on the mirror plane. Iron and magnesium are generally disordered over the two M sites but at low temperature there is a kinetically hindered tendency to order with iron preferentially occupying the M2 octahedera. This effect has been studied using *in*

situ neutron diffraction and the degree of order can be used as an indicator for cooling rate (e.g. Redfern et al., 1996; Redfern, 1998). The structure can accommodate a range of other cations. For example, calcium is partitioned onto the M2 site to form monticellite ($CaMgSiO_4$) and manganese, cobalt and nickel olivines can be synthesised. There are also a range of isostructural materials with technological applications. Examples include the olivine phosphates such as $LiFePO_4$ and $LiCoPO_4$ which are part of a family of materials with potential applications as cathodes in batteries (Chung et al., 2002; Islam et al., 2005).

Because of the technological, geological and basic scientific interest in diffusion in olivine there has been a large number of experimental studies that give the diffusion rate of a number of cations in olivine of various compositions. Experimental data includes a series of studies of silicon diffusion (Béjina and Jaoul, 1996; Béjina et al., 2003; Dohmen et al., 2002; Houlier et al., 1988; Sockel et al., 1980) and many studies of the diffusion of the M site cations including magnesium (Bertran-Alvarez et al., 1993; Chakraborty et al., 1994; Sockel and Hallwig, 1977; Sockel et al., 1980), iron (Bertran-Alvarez et al., 1993; Chakraborty, 1997; Jaoul et al., 1995; Nakamura and Schmalzried, 1984) and cobalt (Morioka, 1980). When considering magnesium diffusion, these experiments can be separated into two types, those that measure tracer diffusion by diffusing ^{26}Mg into an olivine sample of normal isotopic composition and those that measure the interdiffusion of magnesium and another element between two olivine samples of different chemical compositions. The tracer experiments should yield results close to the true self-diffusivity of magnesium in olivine (there is only a small relative mass difference between ^{26}Mg and the normal ^{24}Mg isotope) while interdiffusion experiments yield some average of

the diffusivities of the two diffusing elements in olivine with an intermediate composition (see Chakraborty, 1997, for a quantitative discussion).

The most complete set of tracer diffusion experiments is that of Chakraborty et al. (1994) who performed experiments on synthetic crystals of forsterite as well as natural samples of San-Carlos olivine ($Fo_{\approx 90}$) at temperatures between 1000 and 1300 °C under conditions of controlled oxygen fugacity (pO_2). They give activation energies for magnesium diffusion along [001] of 400($\pm$60) kJmol^{-1} in forsterite and 275($\pm$25) kJmol^{-1} in San Carlos olivine and find that cation diffusion is slower along [010] and [100]. However, no activation energies in the slow directions are reported. Magnesium diffusivity in San Carlos olivine was found to vary with pO_2, in fact the diffusivity was found to be directly proportional to $pO_2^{1/6}$. This result, which is in fair agreement with previous studies (e.g. Nakamura and Schmalzried, 1984, who found diffusivity to be proportional to $pO_2^{1/5.5}$), suggests that the diffusing species is a magnesium vacancy charge balanced by the formation of electron holes or by the oxidation of iron. However, this does not rule out the possibility of diffusion of magnesium interstitial ions formed with a charge neutrality condition involving magnesium vacancies and singly charged oxygen vacancies (Stocker and Smyth, 1977). Intriguingly, in the synthetic olivine, the effect of pO_2 is less clear, with different samples giving different results. Two possibilities were put forward, the first invoking a pO_2 dependent change in the mechanism, and the second invoking interstitial Fe(III) ions in the charge neutrality condition. The effect of pressure on magnesium diffusion was also studied and the activation volume was found to be small and positive (about 1 cm^{3}mol^{-1}), which is similar to the value derived from interdiffusion experiments (Bertran-Alvarez et al., 1993; Jaoul et al., 1995).

Interdiffusion experiments are undertaken by placing two crystals of differing composition together and studying the process by which the two samples approach chemical equilibrium. Two relevant studies are those of Jaoul et al. (1995) and Chakraborty (1997) who studied interdiffusion at 600 – 900 °C and 980 – 1300 °C, respectively. Jaoul et al. (1995) performed their experiments at pressures between 0.5 and 9 GPa in piston-cylinder and multi-anvil apparatus, extrapolated their data to 0 GPa and Fo_{100} composition, and extracted an activation energy for cation diffusion of 147±58 kJmol^{-1} along [010]. The experiments at higher temperature (Chakraborty, 1997) yielded an activation energy for cation diffusion along [001] of 226±18 kJmol^{-1} for olivine of composition Fo_{86}. Recent experiments, using a new thin film based diffusion couple, give activation energies around 200 kJmol^{-1} for Fe-Mg interdiffusion along all three directions (Dohmen et al., 2007).

The effect of dissolved water on cation diffusion in olivine has recently also received attention. Experiments by Wang et al. (2004) and Hier-Majumder et al. (2005) show that magnesium diffusion is at least an order of magnitude more rapid in olivine containing hydrogen that anhydrous olivine of the same composition. However, the activation energy for Fe-Mg interdiffusion between Fo_{90} and Fo_{80} along [001] was measured as 220±60 kJmol^{-1}, little different from that measured in anhydrous experiments (see Figure 7 of Hier-Majumder et al., 2005).Although this large body of experimental data is useful for describing the diffusion controlled processes mentioned above, it does not by itself allow the nature of the point defects or the detailed mechanisms by which they move to be determined. In this regard the inherent resolution of atomic scale computer modelling is a particularly useful approach which can yield crucial details of the key processes leading to diffusion. Armed with such

an understanding we will be in a much better position to gauge the degree to which experimental data can safely be extrapolated.

2 Methodology

We make use of two complementary methodologies to study defects and diffusion on the magnesium sub-lattice of forsterite. First, the formation energies of isolated point defects are studied utilising the Mott-Littleton method with a parameterised potential model (Catlow, 1977b; Sanders et al., 1984; Lewis and Catlow, 1985). These calculations were undertaken employing the GULP code (Gale, 1997; Gale and Rohl, 2003). Further details of the parameters and computational method used can be found in our previous publication on oxygen diffusion in olivine (Walker et al., 2003). These parameters, derived empirically from experimental data for simple binary oxides (supplemented by quantum mechanical data for the oxygen – oxygen interactions), have been successfully used for the modelling of the bulk (e.g. Price et al., 1987; Catlow and Price, 1990) and defect (e.g. Wright et al., 1994; Jaoul et al., 1995; Richmond and Brodholt, 2000; Walker et al., 2005) properties of forsterite and of a wide range of other silicates. Selected results are then validated using an embedded cluster method. This second method involves modelling the defective crystal using a quantum mechanical (QM) description of the electronic structure of the defect and its immediate surroundings coupled to a parameterised molecular mechanical (MM) model of the crystal further from the defect.

For the embedded cluster (QM/MM) calculations we made use of the GUESS code (Sushko et al., 2000b,a) following the recipe described in Braithwaite et al. (2002, 2003), Walker et al. (2006) and Berry et al. (2007). Briefly, the

simulation consists of a small inner QM cluster containing 43 ions when no defects are present, which is embedded within a MM nanocluster of radius 30 Å. In these calculations the inner QM cluster is described using a either Hartree-Fock, Density Functional, or a hybrid B3LYP Hamiltonian using the Gaussian98 package (Frisch et al., 1998). The MM nanocluster is modelled using a potential model fitted to be consistent with the QM charges and all atoms (QM and MM) within 12 Å of the center of the model are allowed to relax to an energy minimum.

The methodology for studying magnesium diffusion by the vacancy mechanism was identical to that described for oxygen diffusion (Walker et al., 2003) – we define possible paths that a magnesium ion could take between adjacent M sites and perform a series of constrained geometry optimizations with the ion held fixed on this path (between two magnesium vacancies). These calculations are then used to determine a starting geometry for a transition state search algorithm based on the Rational Function Optimization (RFO) procedure described by Banerjee et al. (1985) and implemented in GULP. (A starting point close to the transition state is needed in order to avoid the optimizer locating other, less relevant, transition states.) The energy of the defects away from their equilibrium positions is evaluated using the Mott-Littleton method and we break diffusion down into a series of "hops" between adjacent sites. Each hop is associated with a migration energy barrier. By making a series of hops, the diffusing ion may cross the unit cell. Under the assumption that consecutive hops are uncorrelated, the maximum migration energy required to achieve movement in a particular direction is the activation energy for diffusion in that direction. In order to go beyond the activation energy and extract the diffusion coefficient would require dynamical information that could be

obtained from lattice dynamics coupled with Vineyard theory (e.g. Vočadlo et al., 2006). But for a low symmetry structure such as forsterite, further kinetic Monte Carlo analysis of the results would be required.

Because of the apparent complexity of the potential energy surface discovered in the search for the geometry of magnesium interstitial defects described in section 3.2, a different approach was used for interstitial diffusion. The general approach is similar; the potential energy surface is first mapped to locate approximate saddle points and then an RFO transition state search is performed, but the method of locating the approximate saddle point is different. Rather than predetermining individual steps for diffusion, a large segment of the potential energy surface corresponding to moving the interstitial magnesium ion and relaxing the rest of the structure was evaluated. This required 2000 separate Mott-Littelton calculations which were completed in parallel using emerging grid computing technology. In particular we make use of the large Condor pool at University College London (Wilson et al., 2004), which harnesses hundreds of teaching computers to provide a significant high throughput computing resource. Transition states on this surface are then located using an iterative basin filling methodology. The approach, described in more detail by Woodley and Walker (2007), involves the location of the global minimum followed by incrementally increasing an excess energy and determining for the volume a diffusing ion with this energy can sample. When this accessible volume first includes a neighboring periodic image of the global minimum, a transition state and energy barrier is located.

3 Results

3.1 Magnesium vacancies

Using the Mott-Littelton method, the formation energy (energy associated with removing a single ion from the lattice to an isolated state) of a vacancy on the M1 site is calculated as 24.5 eV while the formation energy of an M2 vacancy is 26.4 eV. This means that essentially all magnesium vacancies should form on the M1 site and the energy difference is in good agreement with previous calculations using interatomic potentials and periodic Density Functional Theory (Brodholt, 1997).

The embedded cluster calculations, which are limited to calculations of the M1 vacancy, are in good agreement with the Mott-Littleton results, with calculated defect energy approximately 0.5 eV lower than the Hartree-Fock (HF) result. This agreement is hardly surprising given that magnesium is an ionic species in forsterite. Mulliken population analysis of the electron density gives charges in the region of +2 electronic units, and the parameterised potential is a good description of a formally charged, spherical closed shell ion.

The embedded cluster calculations show few basis set truncation effects (Table 1); explicit relaxation with a 6-31+G* or 6-311+G* basis set (Foresman and Frisch, 1996, give an outline of the meaning of these codes) alters the calculated energy by less than 0.1 eV. Calculations using the HF approximation give the lowest defect energy while DFT with the PW91 functional gives the largest defect energy (almost 1 eV higher in energy than the HF result) suggesting that correlation effects tend to increase the binding of Mg to the

forsterite lattice. As expected, the B3LYP hybrid functional yields intermediate energies.

3.2 Interstitial defects

In practical terms, while vacancies are created by simply removing the relevant ion from the simulation cell more effort is required to establish the structure of interstitials. In the case of interstitial magnesium, location of energy minima was far from straightforward. Initial calculations with interstitial magnesium ions in either of the two vacant octahedral sites resulted in very large ionic displacements on relaxation and final defect energies that were very sensitive to the initial geometry. This is an indication of a failure of the geometry optimisation procedure, probably due to a starting configuration away from an energy minimum on a complex energy hypersurface. In order to locate the minimum energy configuration for a magnesium interstitial, a large number of starting geometries were created by placing interstitial magnesium ions on a regular 0.5 Å grid across the symmetry irreducible portion of the unit cell and performing an optimisation of all atomic coordinates (including the location of the interstitial) using the UCL Condor pool. Following removal of unphysical structures, where the Coulombic attraction between oxygen ions and magnesium ions had overcome the short range repulsion leading to very large negative energies, the lowest energy structures were examined. The low energy configurations were all split interstitials, where the interstitial ion and a displaced lattice magnesium ion were located close to opposite faces of an M1 or M2 octahedron. Embedded cluster calculations show that the split interstitial is substantially more stable (4.4 eV lower in energy) than an oc-

tahedrally co-ordinated magnesium interstitial on the I1 site. The reason for the preference for tetrahedrally co-ordinated magnesium split interstitial defects over octahedrally coordinated interstitial defects on the I1 or I2 site is not immediately obvious on structural grounds. However, at least part of the destabilization of octahedral interstitials is due to electrostatic interactions between the interstitial and the rest of the crystal, which is best described by the electrostatic potential on the site. We find that this is positive which explains the low stability of a positively charged magnesium ion on the site and accounts for the stability of negatively charged, octahedrally coordinated oxygen interstitials (Walker et al., 2003).

The lowest energy site was chosen for further investigation and Mott-Littleton and embedded cluster calculations were set up with the structure (with two interstitial ions and a vacancy) as input. The Mott-Littelton approach gave a formation energy of -17.75 eV and the embedded cluster calculations give similar values, reported in Table 2. Details of the structure derived from the embedded cluster calculation is shown in Figure 2. The two magnesium ions form a split interstitial across the M1 site orientated in the [010] direction with each magnesium ion in distorted tetrahedral co-ordination, in agreement with the structure from the Mott-Littleton calculations. The Mg – O bond distances are similar to those found in crystals with structural magnesium tetrahedrally co-ordinated by oxygen. For example in a recently synthesised bismuth magnesium vanadate (Uma and Sleight, 2002) tetrahedral Mg – O bonds are ∼1.95 Å long, and in the tetragonal Mg_2TiO_4 spinel bond lengths are 1.995 and 1.981 Å (Millard et al., 1995). In the split interstitial defect the bonds are 1.89, 2.02, 1.96 and 1.86 Å long for the Mg – O3a, Mg – O1, Mg – O3b and Mg – O2 bonds, respectively.

The energies of the magnesium split interstitial defect calculated using the QM/MM method and shown in Table 2 are in excellent agreement with the Mott-Littleton methodology. The HF approximation predicts defect energies almost 1 eV higher than DFT, while B3LYP and GGA DFT agree to within better than 0.05%. The Mott-Littleton results fall between those of HF and DFT. Convergence with basis set size is not as good as in the case of the magnesium vacancy (perhaps due to the partial occupation of d-orbitals not represented in the smaller basis sets), but in any case the change in energy from the 6-31+G*//6-31-G to 6-311+G*//6-311+G* is only about 0.1 eV.

3.3 Diffusion

In order to study vacancy diffusion we first defined paths between all adjacent M sites in the olivine structure. Figure 3 shows the five inequivalent routes between magnesium vacancies that we consider may be involved in magnesium vacancy diffusion. Hop A is between two M1 sites along [100] through the vacant octahedral I1 interstitial position while hop B is between two M2 sites along [100] through the vacant octahedral I2 position. Hop C is between two M2 positions with displacement mostly within an (001) plane. Hops D and E are from M1 sites to M2 sites with D mostly within the (100) plane and E with significant components in all three crystallographic directions. Hops D' and E' are the reverse hops from M2 sites to M1 sites. Hop F is between two M1 sites along [001].

Migration energies for each of these hops is given in Table 3, in addition the transition states for interstitial diffusion are also shown. There are several points to note. First, the large barriers to diffusion through the vacant I1 and

I2 octahedra (hops A and B) is somewhat surprising given the expectation that magnesium "prefers" an octahedral environment, and especially given that the transition state is found to be in close to the centre of the octahedron. It seems likely that this is a Coulombic effect that is also responsible for the lack of stable octahedrally co-ordinated magnesium interstitials (as described in section 3.2, above). Vacancy diffusion along [001] is predicted to be via hop F with the low activation energy of 0.72 eV and diffusion along [100] and [010] is predicted to be via hops D and C with a extrinsic activation energy controlled by hop D with a value of 1.98 eV. This is a lower barrier then that found for interstitial diffusion. Therefore interstitial diffusion is not favoured over vacancy diffusion in any direction. The energy barrier for hop F has also been calculated by Béjina et al. (2008) using periodic density functional theory. These calculations give an upper bound on the barrier hight of 0.84 eV, showing that at least this energy barrier is well modeled by the force field model.

4 Discussion

The defect formation energies presented in the preceding sections represent the internal energy contribution needed to remove an ion from the lattice to the gas phase, and to bring an ion from the gas phase, to form vacancies or interstitials, respectively. Thus this energy does not represent any real process. However, before considering more realistic defect reactions, we first address the accuracy of the calculations. As far as we are aware, there is no experimental data that directly constrains defect thermodynamics although some studies give important insights. Instead of considering agreement with experiment,

the consistency of the present results with previous computational studies will be considered. Results from the potential model presented in Table 4 (which includes a summary of the results of this paper) are in excellent agreement with previous work using the same potential model, this includes work that utilised the super-cell approach (Richmond and Brodholt, 2000) as well as the Mott-Littleton method used here (Wright and Catlow, 1994; Jaoul et al., 1995). This is hardly surprising – indeed disagreement would have suggested errors in one or more of the codes used to perform the calculations. An additional test of the accuracy of the potentials based defect energetics is by comparison with the results of electronic structure calculations. In general, as was pointed out in the results sections, good agreement with such calculations is observed. In particular the defect formation energies calculated using the embedded cluster methodology by Braithwaite et al. (2002, 2003), as well as the additional results presented here, are in general agreement with the calculated atomistic values. Discrepancies between results obtained using the potential model and electronic structure methods, and between results from the embedded cluster method and periodic DFT calculations, have been noted by Braithwaite et al. (2003) and Brodholt (1997). The largest error is associated with the formation of a vacancy on the silicon site. The first reason for this error is likely to be that the potential model is unable to describe the resultant five co-ordinate silicate species. A second consideration is that the charge on the silicon vacancy is the largest considered – resulting in the largest correction terms for the long-range polarization and the largest electronic polarisation, especially of the oxygen ions. It is possible that the basis set is not sufficient for modelling this polarisation. Although some of this difference can be attributed to the small size of the super-cell it is likely that an additional factor is caused by the way electronic polarisation around the defect is treated in the atomistic and density

functional calculations. In the DFT study it is likely that the polarisation is under-estimated around the highly charged silicon vacancy because of an inadequate plane wave basis that was only converged with respect to bulk olivine (this would destabilise the defect, as it would have a larger effective charge). On the other hand, the simple shell model used in our potential based calculations could easily overestimate the polarization of oxygen close to the defects, which would tend to make the defects too stable.

Some additional energies are needed in order to consider the defect reactions, these include the enthalpy of formation of a number of minerals that will be the source or sink of the ions from the defect and a number of other standard energies. These are given in Table 4, with formation energies calculated using the same interatomic potential model used to calculate the defect structures and energies.

Crystals at thermodynamic equilibrium contain a number of point defects because the entropy gained in forming the defects outweighs the energetic penalty of forming the defect. For simple uncharged defects the defect concentration at a given temperature can be calculated in a straightforward manner. First the the free energy change in terms of the enthalpy of the formation of the point defect and the configurational entropy gained as a function of defect concentration is explicitly expressed. Then this expression is differentiated to find the minimum free energy, giving the equilibrium defect concentration. Such a procedure is much more complex in multi-component ionic systems because there are a range of possible defect types. In principle one should minimise the free energy numerically, taking into account the enthalpic and entropic contribution from all possible defect species under an imposed condition of charge neutrality (Ashcroft and Mermin, 1976). The first stage requires the

calculation of possible reactions resulting in the formation of intrinsic defects, which is undertaken here. Using the results of the Mott-Littleton calculations gives the energy of a full Schottky defect where a full formula unit of forsterite vacancies is formed and the ions are moved to the surface as:

$$Si_{Si}^{\times} + 2Mg_{Mg}^{\times} + 4O_{O}^{\times} \longrightarrow V_{Si}^{''''} + 2V_{Mg}^{''} + 4V_{O}^{\bullet\bullet} + Mg_2SiO_4 \quad (1)$$

$$E = E(V_{Si}^{''''}) + 2(2V_{Mg1}^{''}) + 4E(V_{O3}^{\bullet\bullet}) + U_{Mg_2SiO_4} = 35.44eV$$

or 5.06 eV per defect. This can be compared with a value of 30.25eV given by GGA calculated using a super-cell containing 56 atoms (Brodholt, 1997). Additional calculations using the same potentials and a fully converged super cell gives better agreement with the Mott-Littleton calculations (36.4 eV). Decreasing the size of the super cell will tend to reduce this value explaining the discrepancy.

The second major type of intrinsic defect is the Frenkel defect where a vacancy is charge balanced by an interstitial of its own type. In principle, Frenkel defects can form on any of the three sublattices. The oxygen Frenkel:

$$O_{O}^{\times} \longrightarrow O_{I}^{''} + V_{O}^{\bullet\bullet} \quad (2)$$

$$E = E(O_{I2}^{''}) + E(V_{O3}^{\bullet\bullet}) = 8.43eV$$

gives a defect energy of 4.22 eV per defect formed, while the magnesium Frenkel:

$$Mg_{Mg}^{\times} \longrightarrow Mg_{I}^{\bullet\bullet} + V_{Mg}^{''} \quad (3)$$

$$E = E(Mg_{I-split}^{\bullet\bullet}) + E(V_{Mg1}^{''}) = 6.73eV$$

yields an energy of 3.37 eV per defect, and the silicon Frenkel defect gives:

$$Si_{Si}^{\times} \longrightarrow Si_I^{\bullet\bullet\bullet\bullet} + V_{Si}^{''''} \tag{4}$$

$$E = E(Si_I^{\bullet\bullet\bullet\bullet}) + E(V_{Si}^{''''}) = 24.21eV$$

or 12.10 eV per defect. Clearly the Mg Frenkel defect will be the predominant intrinsic defect, in agreement with the suggestion of Smyth and Stocker (1975), but this does not rule out the possibility of other intrinsic defects (indeed they are required to minimise the free energy).

The migration energies presented in section 3.3 equate to activation energies for extrinsic diffusion (in the classical sense), and are within error of the experimental results of Jaoul et al. (1995), after their pO_2 correction. For intrinsic diffusion (pure Mg_2SiO_4 with thermally created point defects) an appropriate defect formation energy must be added. Our results suggest that the appropriate defect reaction is the magnesium Frenkel defect, and 3.37 eV should be added to the predicted migration energies to yield the intrinsic activation energy. This results in activation energies of 5.35 eV (513 kJmol^{-1}) along [100] and [010] and 4.09 eV (393 kJmol^{-1}) along [001], which is within the stated error of the results of Chakraborty et al. (1994) for higher temperatures where intrinsic diffusion may be expected. The sense of the anisotropy in activation energy is also correctly described although no experimental results for the activation energy along the slow directions have been presented.

For iron bearing olivine Chakraborty et al. (1994) extracted significantly lower activation energies, presumably because the magnesium vacancies are formed at lower energetic cost. One way to form magnesium vacancies is to charge balance their formation with the oxidation of iron, or by the incorporation of

ferric iron. Using energies of iron defects calculated by Walker et al. (2003), this process can be represented by the reaction:

$$Fe_2O_3 + 3Mg^{\times}_{Mg} \longrightarrow 2Fe^{\bullet}_{Mg} + V''_{Mg} + 3MgO \quad (5)$$

$$E = 2E(Fe^{\bullet}_{Mg}) + E(V''_{Mg}) + 3U(MgO) - U(Fe_2O_3) = 4.47eV$$

In the mantle, it would be more realistic for excess MgO to react with pyroxene to form olivine:

$$Fe_2O_3 + MgSiO_3 + 3Mg^{\times}_{Mg} \longrightarrow 2Fe^{\bullet}_{Mg} + V''_{Mg} + 3Mg_2SiO_4 \quad (6)$$

$$E = 2E(Fe^{\bullet}_{Mg}) + E(V''_{Mg}) + 3U(Mg_2SiO_4) - U(Fe_2O_3) - 3U(MgSiO_3) = 3.81eV$$

Adding one third of these energies (1.49 or 1.27 eV) to the [001] migration energy yields a predicted activation energy of 2.21 or 1.99 eV (213 or 192 kJmol^{-1}), respectively. This is a little lower than the 275±25 kJmol^{-1} measured for tracer diffusion by Chakraborty et al. (1994).

5 Conclusions

The calculations reported here point to a number of interesting results. First, in pure forsterite the majority intrinsic defect species is predicted to be the magnesium Frenkel defect. This does not rule out the possibility of defects on the silicon or oxygen lattices – indeed these are required at equilibrium – but does indicate that electrical conductivity, for example, may be controlled by these defects. There has been at least one theoretical study of the intrinsic conductivity of forsterite (Morin et al., 1977, 1979), this analysed the likely introduction of bands in the band gap in forsterite on the basis of a comparison

with MgO and quartz. The conclusion was that intrinsic conductivity can be explained by postulated magnesium interstitials on the unoccupied octahedral site. The results given above suggest that such defects do not exist and instead the split interstitial defect should predominate; the need for a re-evaluation of intrinsic conductivity data is therefore suggested. In any case, electrical conductivity of olivine under mantle conditions is likely to be controlled by hydrogen diffusion, which is one reason for the major interest in hydrogen speciation in upper mantle rocks. In addition to the energies of defects in forsterite, the defect states in the surrounding minerals should be considered along with the temperature and pressure. Such an analysis is beyond the scope of the current work, but the importance of the oxidation and reduction of iron in the lattice is established.

A further interesting observation is that oxygen ions are able to form interstitial defects in the vacant octahedral sites in the olivine structure but, perhaps surprisingly, magnesium ions are unstable in this environment. The reason for this seems to be at least partially due to the electrostatic interactions between the defect and the rest of the crystal, best described by the electrostatic potential on the site. This is positive, so negatively charged oxygen ions are stabilised by the electrostatic potential while positively charged magnesium ions on the site are penalised.

The results for magnesium diffusion are in agreement with previous computational studies Jaoul et al. (1995) and agree to a remarkable degree with the experimental data. The data of Jaoul et al. (1995) and Chakraborty et al. (1994) for magnesium diffusion in San Carlos olivine can be interpreted as the diffusion of magnesium vacancies charge balanced by iron(III) (with the iron oxidation either corrected to extract "true" extrinsic activation energies

or included in the calculation of the activation energy). The higher activation energy measured by Chakraborty et al. (1994) in synthetic forsterite seems to indicate that true intrinsic diffusion, with magnesium Frenkel defects providing the source of vacancies, was measured in that case. The diffusion of magnesium interstitials is not favoured over vacancy diffusion, a conclusion reinforced by the many measurements of positive pO_2 dependence of magnesium diffusion in olivine.

6 Acknowledgments

A.M.W. acknowledges the receipt of a studentship from the Engineering and Physical Sciences Research Council and K.W. thanks the Royal Society for a University Research Fellowship.

References

Ashcroft, N. W., Mermin, N. D., 1976. Solid State Physics. Saunders College, Orlando.

Banerjee, A., Adams, N., Simons, J., Shepard, R., 1985. Search for stationary points on surfaces. Journal of Physical Chemistry 89 (1), 52 – 57.

Béjina, F., Jaoul, O., 1996. Silicon self diffusion in quartz and diopside measured by nuclear micro-analysis methods. Physics of the Earth and Planetary Interiors 97, 145 – 162.

Béjina, F., Jaoul, O., Liebermann, R. C., 2003. Diffusion in minerals at high pressure: a review. Physics of the Earth and Planetary Interiors 139, 3 – 20.

Béjina, F., Blanchard, M., Wright, K., Price, G. D., 2008. A computer simu-

lation study of the effect of pressure on Mg diffusion in forsterite. Physics of the Earth and Planetary Interiors, this issue.

Berry, A. J., Walker, A. M., Hermann, J., O'Neill, H. S., Foran, G. J., Gale, J. D., 2007. Titanium substitution mechanisms in forsterite. Chemical Geology 242, 176 – 186.

Bertran-Alvarez, Y., Jaoul, O., Liebermann, R. C., 1993. Fe-Mg interdiffusion in single crystal olivine at very high pressure and controled oxygen fugacity: technological advances and initial data at 7 GPa. Physics of the Earth and Planetary Interiors 70, 102 – 118.

Braithwaite, J. S., Sushko, P. V., Wright, K., Catlow, C. R. A., 2002. Hydrogen defects in forsterite: A test case for the embedded cluster method. Journal of Chemical Physics 116 (6), 2628–2635.

Braithwaite, J. S., Wright, K., Catlow, C. R. A., 2003. A theoretical study of the energetics and IR frequencies of hydroxyl defects in forsterite. Journal of Geophysical Research Solid Earth 108 (B6), 2284, article number 2284.

Brodholt, J. P., 1997. Ab initio calculations on point defects in forsterite (Mg_2SiO_4) and implications for diffusion and creep. American Mineralogist 82, 1049 – 1053.

Catlow, C. R. A., 1977b. Point defect and electronic properties of uranium dioxide. Proceedings of the Royal Society of London A. 353, 533 – 561.

Catlow, C. R. A., Price, G. D., 1990. Computer modelling of solid-state inorganic materials. Nature 347, 243–347.

Chakraborty, S., 1997. Rates and mechanisms of Fe-Mg interdiffusion in olivine at 980°C - 1300°C. Journal of Geophysical Research 120 (B6), 12317–12331.

Chakraborty, S., Farver, J. R., Yund, R. A., Rubie, D. C., 1994. Mg tracer diffusion in synthetic forsterite and San Carlos olivine as a function of P, T

and fO_2. Physics and Chemistry of Minerals 21, 489 – 500.

Chung, S. Y., Bloking, J. T., Chiang, Y. M., 2002. Electronically conductive phospho-olivines as lithium storage electrodes. Nature Materials 1 (2), 123–128.

Dieckmann, R., 1998. Point defects and transport in non-stoichiometric oxides: solved and unsolved problems. Journal of Physics and Chemistry of Solids 59 (4), 507–525.

Dohmen, R., Chakraborty, S., Becker, H.-W., 2002. Si and O diffusion in olivine and implications for characterizing plastic flow in the mantle. Geophysical Research Letters 29 (21), 2030.

Dohmen, R., Becker, H.-W., Chakraborty, S., 2007. Fe-Mg diffusion in olivine I: experimental determination between 700 and 1,200°C as a function of composition, crystal orientation and oxygen fugacity. Physics and Chemistry of Minerals 34, 389-407.

Foresman and Frisch (1996) Exploring Chemistry with Electronic Structure Methods. 302 pp. Gaussian Inc. Pittsburgh.

Frisch, M. J., Trucks, G. W., Schlegel, H. B., Scuseria, G. E., Robb, M. A., Cheeseman, J. R., Zakrzewski, V. G., J. A. Montgomery, J., Stratmann, R. E., Burant, J. C., Dapprich, S., Millam, J. M., Daniels, A. D., Kudin, K. N., Strain, M. C., Farkas, O., Tomasi, J., Barone, V., Cossi, M., Cammi, R., Mennucci, B., Pomelli, C., Adamo, C., Clifford, S., Ochterski, J., Petersson, G. A., Ayala, P. Y., Cui, Q., Morokuma, K., Malick, D. K., Rabuck, A. D., Raghavachari, K., Foresman, J. B., Cioslowski, J., Ortiz, J. V., Baboul, A. G., Stefanov, B. B., Liu, G., Liashenko, A., Piskorz, P., Komaromi, I., Gomperts, R., Martin, R. L., Fox, D. J., Keith, T., Al-Laham, M. A., Peng, C. Y., Nanayakkara, A., Gonzalez, C., Challacombe, M., Gill, P. M. W., Johnson, B. G., Chen, W., Wong, M. W., Andres, J. L., Head-

Gordon, M., Replogle, E. S., Pople, J. A., 1998. Gaussian 98 (revision a.7).

Gale, J. D., 1997. GULP: A computer program for the symmetry-adapted simulation of solids. Journal of the Chemical Society, Faraday Transactions 93 (4), 629 – 637.

Gale, J. D., Rohl, A. L., 2003. The general utility lattice program (GULP). Molecular Simulation 29 (5), 291 – 341.

Hier-Majumder, S., Anderson, I. M., Kohlstedt, D. L., 2005. Influence of protons on Fe-Mg interdiffusion in olivine. Journal of Geophysical Research 110, B02202.

Houlier, B., Jaoul, O., Abel, F., Liebermann, R. C., 1988. Oxygen and silicon self-diffusion in natural olivine. Physics of the Earth and Planetary Interiors 50, 240 – 250.

Islam, M. S., Driscoll, D. J., Fisher, C. A. J., Slater, P. R., 2005. Atomic-scale investigation of defects, dopants and lithium transport in the $LiFePO_4$ olivine-type battery material. Chemistry of Materials 17, 5085 – 5092.

Jaoul, O., Bertran-Alvarez, Y., Liebermann, R. C., Price, G. D., 1995. Fe-Mg interdiffusion in olivine up to 9 GPa at T = 600-900°C; experimental data and comparison with defect calculations. Physics of the Earth and Planetary Interiors 89, 199 – 218.

Lewis, G. V., Catlow, C. R. A., 1985. Potential models for ionic oxides. Journal of Physics C: Solid State Physics 18, 1149 – 1161.

Millard, R. L., Peterson, R. C., Hunter, B. K., 1995. Study of the cubic to tetragonal transition in Mg_2TiO_4 and Zn_2TiO_4 spinells by ^{17}O MAS NMR and Rietveld refinement of X-ray diffraction data. American Mineralogist 80, 885 – 896.

Morin, F. J., Oliver, J. R., Housley, R. M., 1977. Electrical properties of

556 forsterite, Mg_2SiO_4. Physical Review B 16 (10), 4434 – 4445.

557 Morin, F. J., Oliver, J. R., Housley, R. M., 1979. Electrical properties of
558 forsterite, mg_2sio_4 II. Physical Review B 19 (6), 2886 – 4445.

559 Morioka, M., 1980. Cation diffusion in olivine - i. cobalt and magnesium.
560 Geochimica et Cosmochimica Acta 44, 759 – 763.

561 Nakamura, A., Schmalzried, H., 1983. On the nonstoichiometry and point
562 defects of olivine. Physics and Chemistry of Minerals 10 (1), 27 – 37.

563 Nakamura, A., Schmalzried, H., 1984. On the Fe^{2+} - Mg^{2+} interdiffusion in
564 olivine (II). Berichte der Bunsen Gesellschaft fr Physikaliche Chemie 88,
565 140 – 145.

566 Price, G. D., Parker, S. C., Leslie, M., 1987. The lattice dynamics of forsterite.
567 Mineralogical Magazine 51, 157 – 170.

568 Redfern, S. A. T., 1998. Time-temperature-dependent M-site ordering in
569 olivines from high-temperature neutron time-of-flight diffraction. Physica
570 B 141, 1189–1196.

571 Redfern, S. A. T., Henderson, C. M. B., Wood, B. J., Harrison, R. J., Knight,
572 S. K., 1996. Determination of olivine cooling rates from metal-cation order-
573 ing. Nature 381, 407 – 409.

574 Richmond, N. C., Brodholt, J. P., 2000. Incorporation of Fe^{3+} into forsterite
575 and wadsleyite. American Mineralogist 85 (9), 1155–1158.

576 Sanders, M. J., Leslie, M., Catlow, C. R. A., 1984. Interatomic potentials for
577 sio2. Journal of the Chemical Society, Chemical Communications.

578 Smyth, D. M., Stocker, R. L., 1975. Point defect and non-stoichiometry in
579 forsterite. Physics of the Earth and Planetary Interiors 10, 183 – 192.

580 Sockel, H. G., Hallwig, D., 1977. Ermittlung kleiner diffusionskoeffizienten
581 mittels SIMS in oxydischen verbindungen. Mikrochimica Acta Suppl. 7, 95–
582 107.

583 Sockel, H. G., Hallwig, D., Schachtner, R., 1980. Investigations of slow ex-
584 change processes at metal and oxide surfaces and interfaces using secondary
585 ion mass spectrometry. Materials science and engineering 42, 59 – 64.
586 Stocker, R. L., Smyth, D. M., 1977. Effect of enstatite activity and oxygen
587 partial pressure on the point-defect chemistry of olivine. Physics of the
588 Earth and Planetary Interiors 16, 145–156.
589 Sushko, P. V., Shluger, A. L., Baetzold, R. C., Catlow, C. R. A., 2000a. Em-
590 bedded cluster calculations of metal complex impurity defects: properties of
591 the iron cyanide in NaCl. Journal of Physics: Condensed Matter 12, 8257 –
592 8266.
593 Sushko, P. V., Shluger, A. L., Catlow, C. R. A., 2000b. Relative energies of
594 surface and defect states: ab initio calculations for the MgO (001) surface.
595 Surface Science 450, 153–170.
596 Tsai, T.-L., Dieckmann, R., 1997. Point defects and transport of matter and
597 charge in olivines, $(Fe_xMg_{1-x})_2SiO_4$. Materials Science Forum 239 - 241,
598 399 – 402.
599 Tsai, T.-L., Dieckmann, R., 2002. Variation of the oxygen content and point
600 defects in olivines, $(Fe_xMg_{1-x})_2SiO_4$, $0.2 \leq x \leq 1.0$. Physics and Chemistry
601 of Minerals 29, 680 – 694.
602 Uma, S., Sleight, A. W., 2002. A new bismuth magnesium vanadate with
603 reduced vanadium: $BiMg_{2.5}V_{18.5}O_{38}$. Journal of Solid State Chemistry 164,
604 138 – 143.
605 Vočadlo, L., Wall, A., Parker, S. C., Price, G. D. 1995. Absolute ionic diffusion
606 in MgO – computer calculations via lattice dynamics. Physics of the Earth
607 and Planetary Interiors 88, 193 – 210.
608 Walker, A. M., 2004. Computational studies of point defects and dislocations
609 in forsterite (Mg_2SiO_4) and some implications for the rheology of mantle

610 olivine. PhD, University of London.

611 Walker, A. M., Demouchy, S., Wright, K., 2006. Computer modelling of the
612 energies and vibrational properties of hydroxyl groups in α- and β-Mg_2SiO_4.
613 European Journal of Mineralogy 18, 529 – 543.

614 Walker, A. M., Gale, J. D., Slater, B., Wright, K., 2005. Atomic scale mod-
615 elling of the cores of dislocations in complex materials part 2: applications.
616 Physical Chemistry Chemical Physics 7.

617 Walker, A. M., Wright, K., Slater, B., 2003. A computational study of oxygen
618 diffusion in olivine. Physics and Chemistry of Minerals 30 (9), 536 – 545.

619 Wang, Z. Y., Hiraga, T., Kohlstedt, D. L., 2004. Effect of H^+ on Fe-Mg in-
620 terdiffusion in olivine, $(Fe,Mg)_2SiO_4$. Applied Physics Letters 85 (2), 209 –
621 211.

622 Wilson, P., Emmerich, W., Brodholt, J., 2004. Leveraging HTC for UK
623 eScience with very large Condor pools: Demand for transforming untapped
624 power into results. In: Proceedings of the UK e-Science All Hands Meeting
625 2004.

626 Woodley, S. M., Walker, A. M., 2007. New software for finding transition states
627 by probing accessible, or ergodic, regions. Molecular Simulation 33, 1229 –
628 1231.

629 Wright, K., Catlow, C. R. A., 1994. A computer simulation study of (OH)
630 defects in olivine. Physics and Chemistry of Minerals 20, 515 –518.

631 Wright, K., Freer, R., Catlow, C. R. A., 1994. The energetics and structure of
632 the hydrogarnet defect in grossular: a computer simulation study. Physics
633 and Chemistry of Minerals 20, 500 – 503.

Table 1

Defect energies for Mg1 vacancies in forsterite calculated using the embedded cluster method. The basis set code refers to the basis used for geometry optimisation and final energy calculation respectively (so 6-31+G*//6-31G means optimisation using the 6-31G basis with final energy calculation using the 6-31+G* basis). Rapid convergence is observed for each method with basis set size.

Basis set	Defect energy (eV)		
	Hartree-Fock	DFT (PW91)	DFT (B3LYP)
6-31G//6-31G	25.832	27.127	26.875
6-31+G*//6-31G	24.942	25.725	25.564
6-31+G*//6-31+G*	24.979	25.762	25.610
6-311+G*//6-31+G*	25.002	25.780	25.632
6-311+G*//6-311+G*	25.017	25.773	25.625

Table 2

Defect energies for the magnesium split interstitial across the M1 site. The meaning of the basis set symbols are given in the caption to Table 1.

Basis set	Defect energy (eV)		
	Hartree-Fock	DFT (PW91)	DFT (B3LYP)
6-31G//6-31G	-18.029	-18.470	-18.478
6-31+G*//6-31G	-17.366	-17.952	-17.947
6-31+G*//6-31+G*	-17.403	-18.001	-17.993
6-311+G*//6-31+G*	-17.503	-18.045	-18.038
6-311+G*//6-311+G*	-17.508	-18.049	-18.043

Table 3

Migration energies for magnesium vacancy and interstitial diffusion in forsterite.

Hop	Defect energy of initial state (eV)	Defect energy of activated state (eV)	Migration energy (eV)
A	24.48	30.37	5.89
B	26.40	35.50(a)	9.10
C	26.40	27.87(a)	1.47
D	24.48	26.46	1.98
D'	26.40		0.06
E	24.48	30.94(a)	4.54
E'	26.40		6.64
F	24.40	25.12	0.72
Interstitial // [100]	-17.75	-13.86	3.89
Interstitial // [010]	-17.75	-13.86	3.89
Interstitial // [001]	-17.75	-14.62	3.13

(a) These failed to converge in the RFO part of the calculation and so an estimate of the transition state is made from the initial search, where the moving ion is fixed and the rest of the structure relaxed, is used, the true energy of the activated state is not expected to be significantly different from this estimate.

Table 4

Defect energies for a range of possible intrinsic defects in forsterite

Defect [a]	Mott-Littleton method (eV)
$V_{O1}^{\bullet\bullet}$	27.97 [b]
$V_{O2}^{\bullet\bullet}$	25.20
$V_{O3}^{\bullet\bullet}$	24.54
$O_{I(1)}''$	-14.37
$O_{I(2)}''$	-16.11
V_{Mg1}''	24.48
V_{Mg2}''	26.40
$Mg_{I(split)}^{\bullet\bullet}$	-17.75
V_{Si}''''	100.81 [c]
$Si_{I}^{\bullet\bullet\bullet\bullet}$	-76.60
$Fe_{M1}^{\bullet}$	-22.55 [d]
$Fe_{M2}^{\bullet}$	-23.24
$U(Mg_2SiO_4)$	-212.49
$U(MgSiO_3)$	-171.97
$U(Fe_2O_3)$	-150.37
$U(MgO)$	-41.31

[a] Defects are described using Kröger-Vink defect notation and include vacancies in all three oxygen positions, oxygen interstitial ions occupying both free octahedral sites on both magnesium sites, a split interstitial magnesium defect, a silicon vacancy and a silicon interstitial. Defect energies are quoted with respect to the perfect forsterite lattice and the ion at infinity.

[b] Energies of oxygen defects are from Walker et al. (2003)

[c] Energies of silicon defects are from Walker (2004)

[d] Energies of iron defects are from Walker et al. (2003)

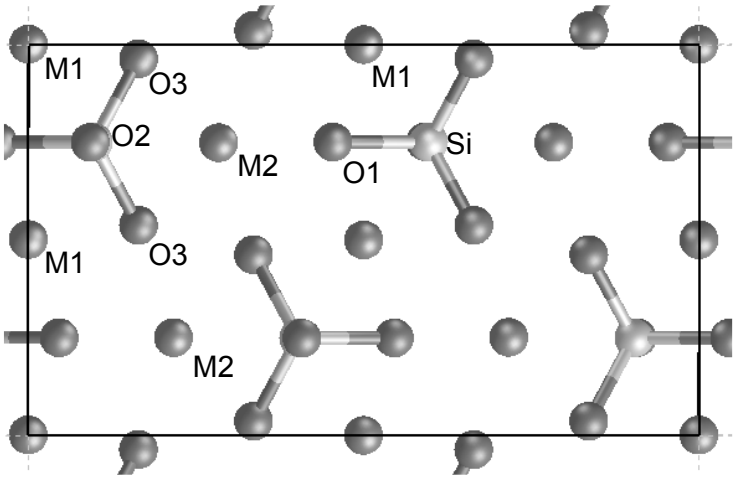

Fig. 1. Unit cell of the olivine structure viewed along [100]. The long visible cell axis is [010] and the shorter one is [001], occupied sites are marked.

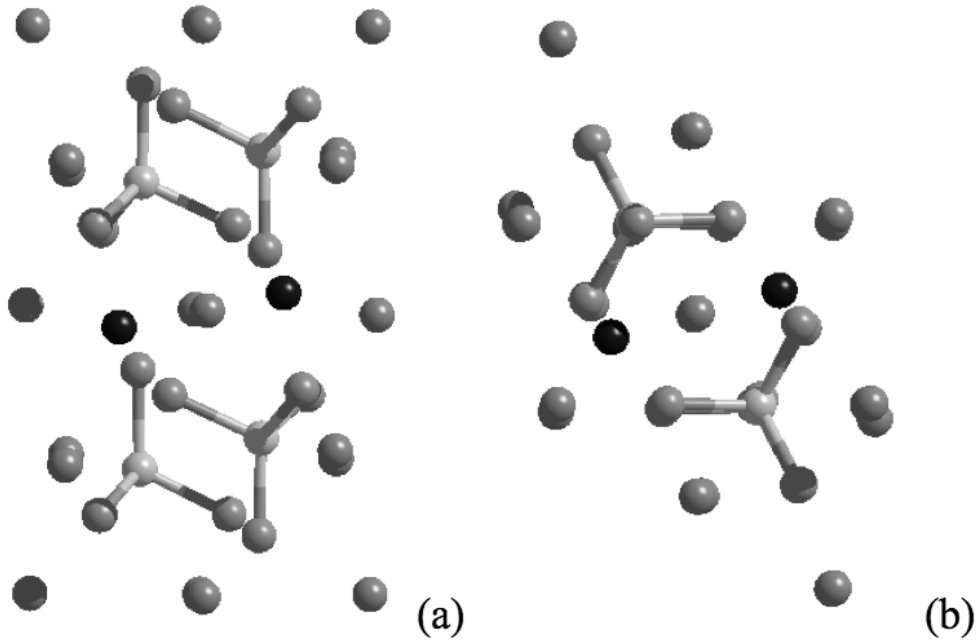

Fig. 2. Structure of magnesium split interstitial defect from embedded cluster calculations. (a) Looking along [010] with [100] oriented up the page. (b) Looking along [100] with [001] oriented up the page. The two tetrahedral magnesium ions are shown in black, otherwise magnesium ions isolated spheres, silicon and oxygen ions form SiO_4 tetrahedra.

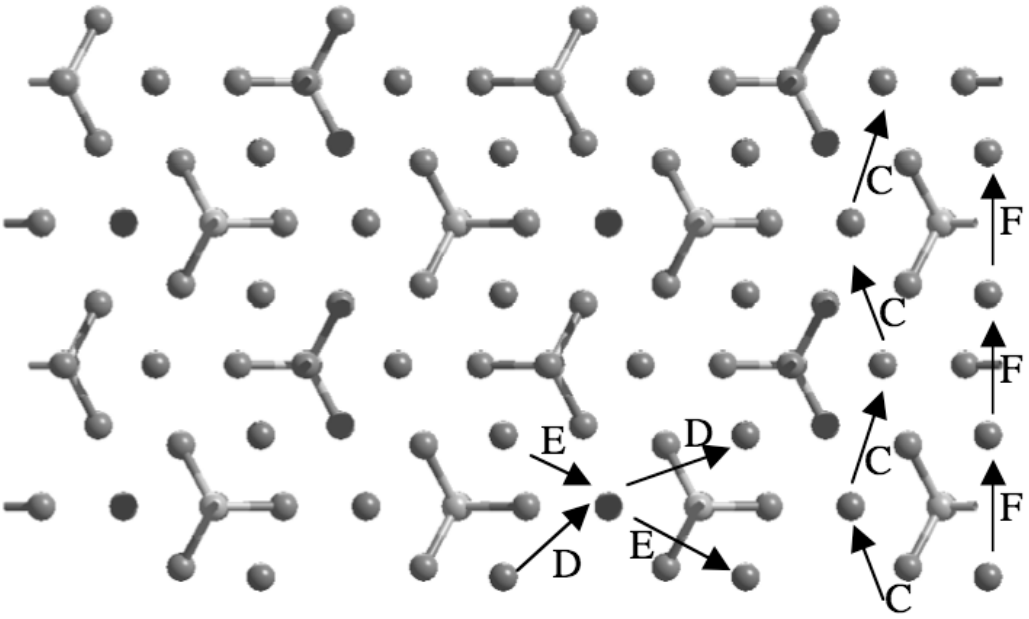

Fig. 3. Magnesium diffusion by the vacancy mechanism (see text for details) projected onto the (100) plane. Hops A and B are not shown as they are perpendicular to the plane.